

Synthesis and Characterization of Hexagonal Prism like Zinc Oxide for Electrochemical Determination of Gallic Acid in Wine Samples

Kesavan Ganesh¹, Allen Joseph Anthuvan², Shen-Ming Chen^{1,}, Kumuthini Rajendran³, Tse-Wei Chen^{1,4}, Viswanathan Chinnuswamy², Shih-Yi Lee^{5,*}, Wen-Han Chang^{6,7,8}*

¹ Electroanalysis and Bioelectrochemistry Lab, Department of Chemical Engineering and Biotechnology, National Taipei University of Technology, No. 1, Section 3, Chung-Hsiao East Road, Taipei 106, Taiwan, ROC.

² Department of Nanoscience and Technology, Bharathiar University, Coimbatore 641 046, India.

³ Nanotechnology Research Centre, SRM Institute of Science and Technology, Chennai 603 203, India.

⁴ Research and Development Center for Smart Textile Technology, National Taipei University of Technology, Taipei 106, Taiwan, ROC

⁵ Division of Pulmonary and Critical Care Medicine, MacKay Memorial Hospital; MacKay Medicine, Nursing and Management College.

⁶ MacKay Memorial College Department of Cardiology, MacKay Memorial Hospital, Taiwan.

⁷ Department of Emergency Medicine, MacKay Memorial Hospital; Institute of Mechatronic Engineering, National Taipei University of Technology, Taiwan

⁸ Graduate Institute of Injury Prevention and Control, Taipei Medical University; Department of Medicine, Taiwan

*E-mail: smchen78@ms15.hinet.net, leesy5538@yahoo.com.tw

Received: 7 January 2019 / Accepted: 25 February 2019 / Published: 10 April 2019

Metal oxides have stimulated significant attention due to their potential applications in various technology and applications. In this paper, facile and novel hexagonal prism like zinc oxide (HP-ZnO) has been successfully synthesized by mechanochemical synthesis. As prepared HP-ZnO was characterized by X-ray diffraction (XRD), scanning electron microscopy (SEM), Energy-dispersive X-ray spectroscopy (EDS), particle size distribution and ultraviolet visible spectroscopy (UV-vis). Moreover, the electrochemical behavior of the proposed electrode was examined by the cyclic voltammetry and amperometric techniques. The electrochemical sensor exhibited a wide linear range from 0.1 to 130 μM with a trace-level detection of 0.02 μM (S/N=3) and showed good linearity $R^2 = 0.9903$. This excellent electrochemical sensing ability can be attributed to good surface area, electronic conductivity and numerous active sites. The practical application of proposed electrochemical sensor was proved by successful detection of GA in wine samples. The results indicated that the HP-ZnO is promising electrochemical sensor for selective determination of GA at trace levels in real samples.

Keywords: Metal Oxides, Amperometric Method, Phenolic Compounds, Gallic Acid, Wine Samples.

1. INTRODUCTION

Gallic acid (GA) is an important and natural phenolic compounds that have been widely available in the blueberry, black rice, grapes, hops, green tea, walnuts, sumac, black tea, and apples [1, 2]. It has a strong biological properties including anti-bacterial, anti-mutagenic, anti-oxidant, anti-viral, anti-cancer, anti-inflammation [3–5]. So, it is of prime importance to accurately detect the GA in day to day life for human health. In such a way, several analytical methods like resonance light scattering, photo electrochemical platform, flow injection analysis, fluorescence, thin-layer chromatography and electrochemical methods [5–10] have been established for detection. Among them, electrochemical techniques have gained the several advantages like excellent sensitivity, trace level detection, good selectivity and rapid response compare with other methods [11–19]. Recent developments in nanomaterial synthesis has paved way for involving alternative approach rather than relying on conventional chemical synthesis routes like solvothermal, hydrothermal, sono-chemical and sol gel method [20–23]. In mechanochemical synthesis, nanoparticles as small as 10 nm can be prepared with desired phase, milling time dependence and in the absence of external temperature [24]. During the milling process, chemical reactions and phase transformation occurs. This method proves to be advantageous for its large-scale production and less processing time. In mechanochemical process the multicomponent complex ceramics, metals and metal oxides can be synthesized in ease with phase purity than any other conventional synthesis methods. Zinc oxide nanomaterials have gained much attention due to its easy synthesis, morphological tuned properties, excellent electron mobility (60 meV) and wide band gap (3.2 eV) [25].

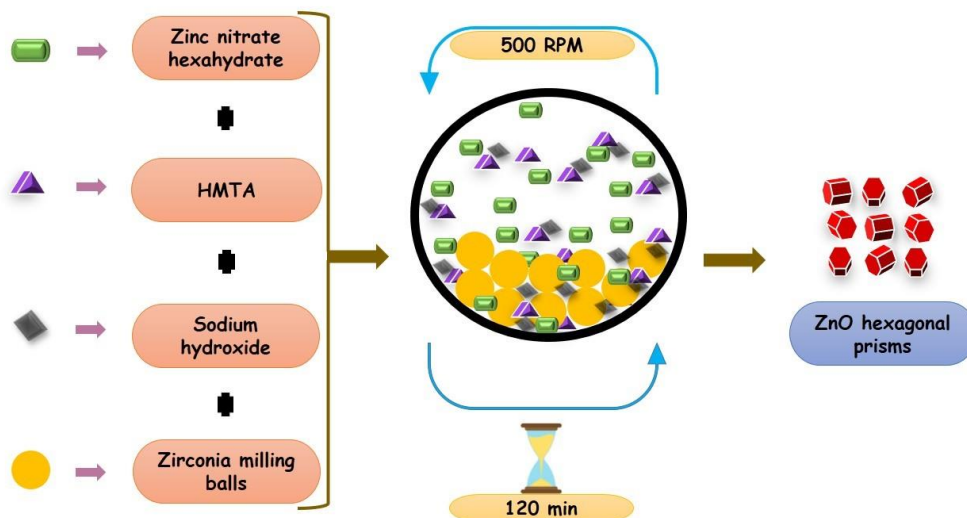
In present study, we are reporting a simple preparation for hexagonal prism like ZnO (HP-ZnO) by mechanochemical milling process with precursors colliding with the milling balls for defined time, then followed by a washing process to remove the unreacted by products and a subsequent heating. The as-prepared HP like ZnO was confirmed by X-ray diffraction (XRD), scanning electron microscopy (SEM), Energy-dispersive X-ray spectroscopy (EDS), particle size distribution and ultraviolet visible spectroscopy (UV-vis). The HP-ZnO modified electrode was examined by the cyclic voltammetry (CV) and amperometric techniques. Fortunately, the HP-ZnO sensor exhibited excellent electrochemical activities toward the determination of GA. All the physiochemical results are evidently proved that the HP-ZnO is more efficient and acceptable electrode for the determination of GA.

2. EXPERIMENTAL SECTION

2.1 Chemicals and Reagents

All chemicals were of analytical grade and utilized without additional purification. Zinc nitrate hexahydrate, hexamethylenetetramine (HMTA), sodium hydroxide and ethanol were purchased from Merck specialties. Gallic acid, mono sodium dihydrogen phosphate (NaH_2PO_4), disodium hydrogen

phosphate (Na_2HPO_4) and sodium hydroxide (NaOH) were received from sigma Aldrich. The 0.05 M phosphate-buffered solution (PBS) (pH 3.0) was used as supporting electrolyte for the all electrochemical studies. The double ionized (DI) water was used for the stock solutions and experiments



Scheme 1 The schematic representation of mechanochemical synthesis HP like ZnO.

2.2 Mechanochemical synthesis of hexagonal prism like ZnO

A typical mechanochemical process was carried out in a typical planetary ball milling (FRITSCH pulverisette 7) with Zirconia bowls of 80 ml volume and 10 mm diameter Zirconia milling balls as accessories for the synthesis of HP-ZnO. Zinc nitrate hexahydrate was used as a zinc precursor, HMTA was used as a surfactant and sodium hydroxide for pH adjustment were used as starting chemicals in the milling process. The chemicals were mixed homogeneously in a ratio of 2: 1 : 0.5 before subjecting to the milling. During mechanochemical milling, the ball and precursor ratio was maintained at 10:1 respectively. Mechanochemical milling was carried out at 500 rpm for 120 min. After milling process, the slurry precursor was collected and washed several times with deionized water and ethanol to remove the unreacted precursor byproducts. The washed sample was vacuum dried at 80°C for 1 hour and calcined in a muffle furnace at 400°C for 2 hours. The final product was stored in a vacuum desiccator.

2.3 Fabrication of HP-ZnO modified electrode

Prior to the electrode modification, the electrode was polished with various sized alumina powder to obtain a clear and mirror like surface. In order to fabricate a modified electrode, 10 mg of HP-ZnO was dispersed in 1 mL of water by 20 min ultrasonic agitation to acquire a uniform suspension. After that, 7.0 μL of the homogeneous HP-ZnO suspension was coated onto the GCE surface and dried at room temperature.

2.4. Characterization

The crystalline nature of synthesized ZnO hexagonal prism HP-ZnO was investigated using X-ray diffraction (X'Pert PRO, PANalytical). The morphological and compositional analysis were performed using Scanning Electron Microscope (Quanta 200, FEI), Dynamic light scattering (nano ZS90, Malvern) and Energy dispersive Spectroscopy (EDAX). UV-Vis absorption spectra and Kubelka-Munk (KM) plot were obtained using UV-Vis spectrophotometer (V-660, JASCO). The electrochemical behavior of the as-prepared material was examined by CH Instruments (*Made in U.S.A*) 750a. All the electrochemical measurements are conducted in the nitrogen atmosphere at room temperature.

3. RESULTS AND DISCUSSION

3.1 Physical Characterization of HP-ZnO

In Fig. 1(A&B), represent the typical morphology of HP-ZnO. Due to enduring repeated collision of balls and precursors for a time period of 120 min followed by heat treatment the nucleation takes place, resulting in the grain growth following the formation of HP-ZnO nanocrystals. The dominant morphology of HP-ZnO was found to be with hexagonal sections with prism like appearance and this coincides with the crystal structure of XRD results.

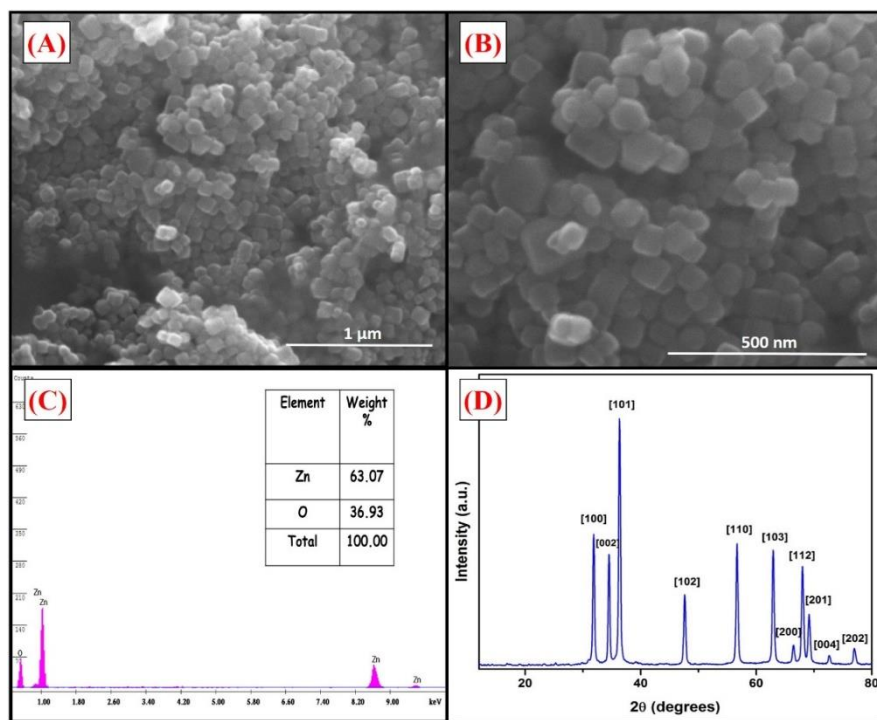


Figure 1. (A&B) Different SEM micrograph, (C) EDX (*Inset*: Elemental percentage), (D) XRD pattern of mechanochemical synthesized HP like ZnO.

In higher magnification image Fig. 1B reveals the aggregated nanocrystals of HP-ZnO was found to be with an average particle size of 200 nm. The particle aggregation was due to the influence of milling time and the ratio of balls to precursor. It was clear that the morphology and size of HP-ZnO can be analyzed distinctively than comparing with previous reports [27]. The EDS spectra in Fig. 1C of HP-ZnO, shows the weight percentage of zinc and oxygen present in the sample. The weight percentage of zinc was found to be 63.07% and for oxygen, it was 36.93%. From the result, it is evident that no other peaks for sodium and carbon was found.

The XRD pattern of mechanochemically synthesized HP-ZnO was depicted in Fig. 1D and it reveals the high crystalline nature of the sample with hexagonal wurtzite structure and matches the standard JCPDS File No: 36-1451. The diffraction patterns were indexed accordingly and the (101) phase was found to be with sharp higher intensity. This result is in accordance with EDS to reveal the purity of the HP-ZnO and the by products are removed while washing. The hydroxide characteristic peaks were absent this suggests the high crystallinity and purity of HP-ZnO. The crystallite size was found using Scherrer's equation [28],

$$D = \frac{k\lambda}{\beta \cos\theta}$$

Where, D is the average crystallite size and λ is the wavelength of the X-ray used (Cu $\alpha_1 = 0.15406$ nm), β is the full width at half of the maximum (FWHM) and θ is the diffraction angle. The average crystallite size was found to be 24 nm.

Table 1. Structural parameters of HP like ZnO calculated from XRD

Parameters	(100) Plane	(002) plane	(101) Plane
θ°	15.94	17.23	18.16
B	0.00612	0.00561	0.00627
D (nm)	23	25	23
d (nm)	28	26	24.7
$\delta \times 10^{15} (\text{Kg m}^{-3})$	1.842	1.527	1.889
$\varepsilon \times 10^{-3} (\text{Kg m}^{-3})^2$	1.47	1.34	1.49
$a = 3.239 \text{ \AA}$			
$c = 5.205 \text{ \AA}$			
$V = 51 \text{ \AA}^3$			

The lattice parameters of the hexagonal structure of mechanochemically synthesized HP-ZnO for the plane (100), (002) and (101) was estimated using the relation,

$$\frac{1}{d^2} = \frac{4}{3} \left[\frac{h^2 + hk + l^2}{a^2} \right] + \frac{l^2}{c^2}$$

where a and c are the lattice parameters, (hkl) is the Miller indices of the particular diffraction peak and d is the inter planar spacing and it is calculated using the Bragg's law. The d spacing value and the lattice parameters are displayed in Table-1. Due to the milling process a shift of 0.03° in 2θ angle and a decrease in lattice parameter values was observed, this may be due to the strain relaxation induced during the synthesis [25].

$$V = \frac{\sqrt{3}}{2} a^2 c$$

$$\delta = \frac{1}{D^2}$$

$$\varepsilon = \frac{\beta \cos \theta}{4}$$

Hence the lattice strain (ε), dislocation density (δ) and volume (V) of unit cell for the hexagonal system [26] were evaluated and displayed in Table-1.

The UV-Vis absorption of HP-ZnO is an important parameter to study its optical properties. From Fig. 2A, it is clear that the absorption band of the HP-ZnO have shifted to red region due to the milling time of 120 min relating with ZnO nanoparticles prepared in previous reports. The UV-Vis absorption band of HP-ZnO is size dependent, hence when the crystallite size is decreased the practically bands have red shift. The red shift is also may be due to the lattice strain caused during the milling process. The band gap of the material is calculated from the Kubelka-Munk (KM) plot obtained from UV-Vis absorption spectra Fig. 2B. In this study the bandgap energy (E_g) of HP-ZnO was evaluated from the plot of photon energy (eV) versus $[F(R)hv]^{1/2}$ and with a slope linear to photon energy the bandgap energy (E_g) was found to be 3.13 eV. The bandgap energy was found to be decreased as a result of lattice strain generated during milling process. From Fig. 2C, the particle size distribution of HP-ZnO reveals the narrow distribution of the nanocrystals with a mean diameter of 220 nm. This narrow distribution of the prominent peak reveals the low degree of aggregation and was found to be in a good match with the particle size estimated form SEM micrographs.

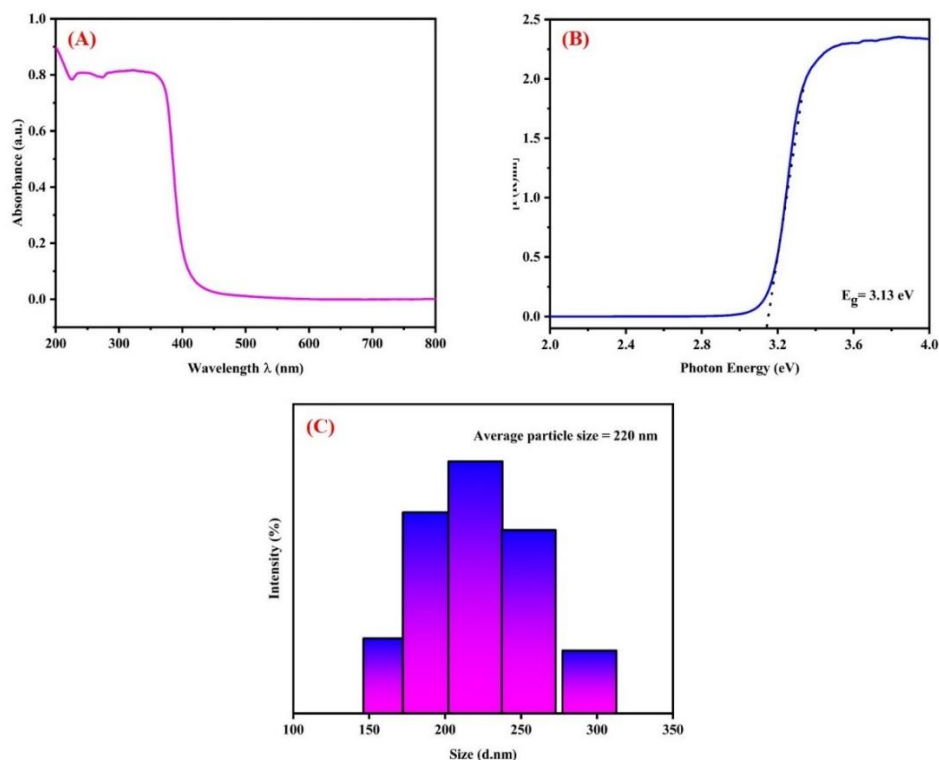


Figure 2. (A) UV-Vis absorption spectra, (B) Kubelka-Munk (KM) plot and (C) Particle size distribution of mechanochemical synthesized HP like ZnO.

3.2. Electrochemical behaviour of GA on the bare and modified electrode

The electrochemical activity of the bare and modified electrodes were first investigated via cyclic voltammetric (CV) technique using the detection of GA. The electrochemical behavior of bare GCE and HP-ZnO/GCE was examined by CV without (a, b) and with (c, d) presence of 200 μM GA containing 0.05 M PBS (pH 3.0) at a scan rate of 50 mV/s (Fig. 3).

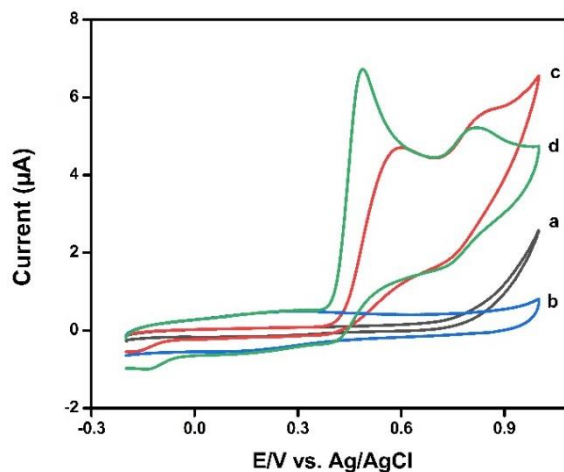
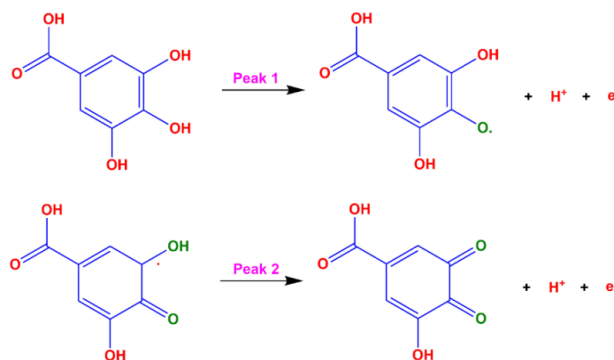


Figure 3. CV response of (a) GCE (b) HP-ZnO in the absence (c) GCE (d) HP-ZnO in the presence of 200 μM of GA containing 0.05M PBS (pH 3.0) at a scan rate of 50 mV/s.

At first, there is no electrochemical signal at un-modified GCE (a) and HP-ZnO/GCE (b) in the absence of GA. Bare GCE shows a weak and sluggish oxidation peak towards GA detection with peak current of 4.69 μA . The HP-ZnO/GCE displayed an excellent electrocatalytic performance in terms of increasing the oxidation peak current ($I_{pa} = 6.8 \mu\text{A}$). When electrode was modified with HP-ZnO, the oxidation peak potential shifted toward the more anodic side and peak current also increased compared with the bare GCE. The onset anodic peak potential of GA were +0.59V and +0.48 (Vs. Ag/AgCl) at the bare GCE and HP-ZnO/GCE, respectively, indicating GA is more easily oxidized at the HP-ZnO modified electrode. Furthermore, the improved GA response is in accordance with the large surface area, enhanced conductivity and rapid electron transfer rate. The possible electrochemical mechanism of the electrochemical pathways shown in Scheme 2.



Scheme 2. The overall electrochemical oxidation mechanism of GA.

3.2.1 Effects of scan rate and pH

In Fig. 4A shows the influence of scan rate on the electrochemical behavior of 200 μM GA at the ZnO modified electrode in 0.05M PBS (pH 3.0) with various scan rate. From the CV curves, the anodic peak currents was gradually increases with different scan rates from 20 to 200 mV/s. A linear relationship between scan rate and peak current is found and the linear equation is expressed: $y = 0.0206x + 4.1107$ ($R^2 = 0.9973$) (Fig. 4B). These obtained indicating the Ga oxidation at ZnO/GCE is dominated by surface-controlled process. The effect of pH values on electrochemical response of 200 μM GA at the ZnO/GCE was examined (Fig. 4C). With varying the pH value of PBS, the proposed electrochemical sensor exhibited different CV profiles. It can be clearly observed that the maximum oxidation anodic current appears at pH 3.0. Additionally, the Fig. 4D shows the bar diagram for the pH values. Hence, the pH 3.0 was further used for the electrochemical measurements of GA.

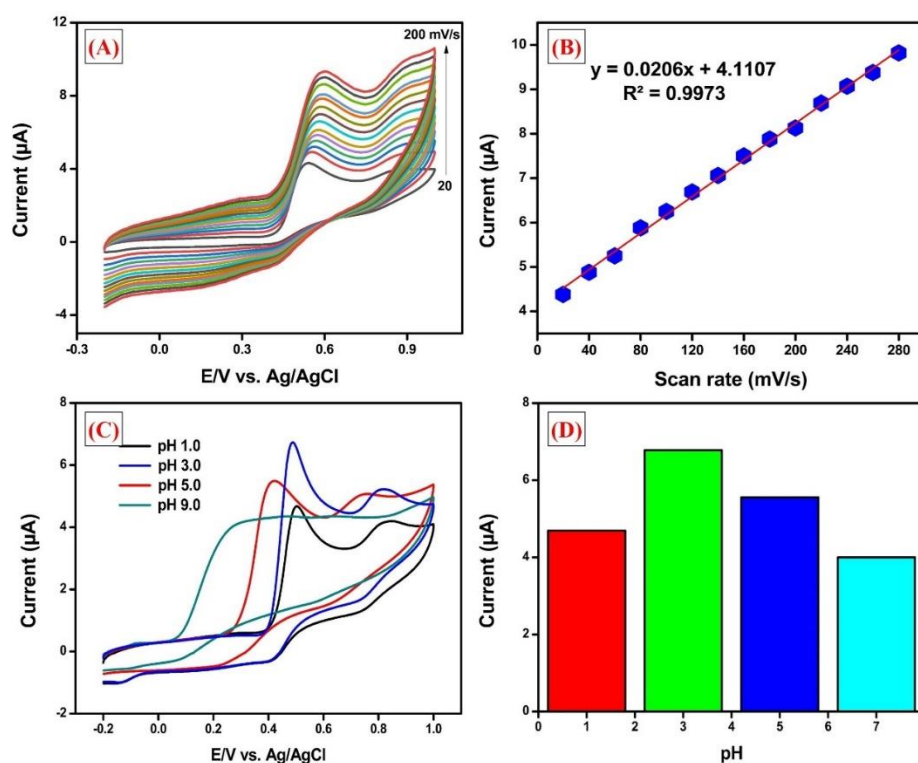


Figure 4. (A) CV curves of GA oxidation on HP-ZnO for various scan rates from 20 to 200 mV/s. (B) The linear calibration plot between peak current and scan rate. (C) CV response of GA on HP-ZnO in various pH ranges from 1.0 to 9.0 containing 0.05M PBS at a scan rate of 50 mV/s. (D) The bar diagram for various pH values.

3.2.2 Amperometric detection of GA

Fig. 5 shows the amperometric response for various concentrations of GA from 0.1 to 1200 μM in in 0.05M PBS (pH 3.0) under applied electrode potential was held at +0.48 V with rotation speed was fixed at 1500 RPM. As expected, the electrochemical oxidation peak currents were increased proportionally with increasing the concentrations of GA, owing to the superior electrocatalytic oxidation activity of ZnO modified electrode. The anodic peak current was plotted against the various

concentration of GA and exposed in Fig. 5 (*Inset*), it exhibits the linearity from 0.1 μM to 130 μM with the linear correlation coefficient of $R^2 = 0.9903$. The detection limit was found to be 0.02 μM ($S/N = 3$). The excellent performance of the electrochemical sensor are directly attributed to the good conductivity, large specific surface area and high active sites of HP-ZnO. The comparisons of ZnO/GCE with other modified electrodes for the electrochemical determination of GA were summarized in Table 2. As shown, the fabricated ZnO sensor in this paper met the clinical requirements of GA detection with a dynamic linear range and low trace level detection compared to the literature [2, 5–13].

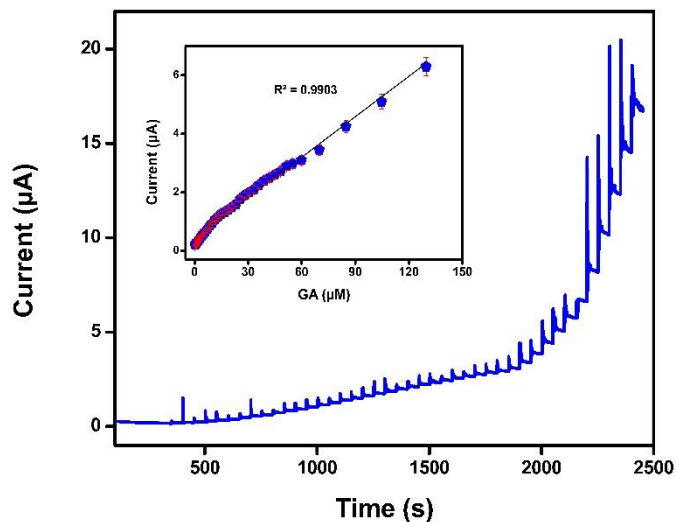


Figure 5. The amperometric response of HP-ZnO with various concentration of GA in 0.05 M PBS (pH 3) (**Inset:** The plots of peak current of GA vs. various concentration).

Table 2. Electrochemical comparison on the performance of HP-ZnO modified electrode with previously modified electrodes towards detection of GA.

Electrodes	Linear range (μM)	LOD (μM)	Ref.
MCPE/CNT	0.5–150	0.3	2
TiO ₂ /CPE	2.5–150	0.94	5
GCE/PEP	1–20	0.06	6
CPE/SiO ₂	0.8–100	0.25	7
CPE/MWCNT-Fe	0.5–15	0.3	8
GCE/SF-GR/AuCM	0.05–8	0.0107	10
Au/MWNT-PDDA	1–10	0.01	11
CS-fFe ₂ O ₃ -ERGO/GCE	1–100	0.15	12
AgNP/Delph/GCE	0.6–8.68	0.28	13
HP-ZnO/GCE	0.1–130	0.02	This work

3.2.3 Selectivity, Reproducibility and Practical Application

The anti-interference ability playing a significant role in newly proposing electrochemical sensors. The amperometric method was used for examine the stability studies in the presence of potentially interfering compounds such as catechol (CT), dopamine (DA), caffeic acid (CA), morin (MR), hydroquinone (HQ), uric acid (UA), ascorbic acid (AA), ferulic acid (FA) and acetaminophen (AC) (Fig. 6A). Notably, the negligible current changes were observed confirming that the ZnO based electrochemical sensor is highly selective towards GA detection. This stability study clearly proved that the ZnO sensor was more suitable for the determination of GA in real samples. The reproducibility of proposed sensor was further explored by sensing GA for five different and freshly prepared electrodes under the same conditions of Fig. 3. As shown in Fig. 6B, the CV response of the proposed sensor towards GA shows relative standard deviation (RSD) of 4.53% for five independent electrodes. For real time monitoring, the practical ability of the proposed ZnO electrochemical based sensor was examined by determining GA in wine samples. The standard addition method was used for examine the recovery percentage of GA and the obtained results were listed in Table 3. It can be seen that the recovery was found to be 99.7–107.0%, suggesting the proposed sensor was possible to determine GA in real samples. These results demonstrated that the ZnO modified electrode had good selectivity, reproducibility and practicability for GA detection.

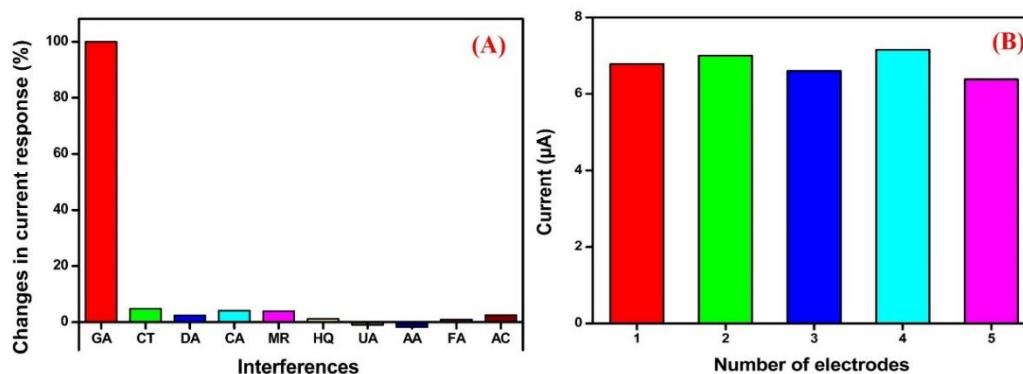


Figure 6. (A) The bar diagram of interference studies and (B) Reproducibility of the HP-ZnO/GCE for five different electrodes.

Table 3. Determination of GA in wine sample (n=3).

Beverage type	Added (μM)	Found (μM)	Recovery (%)	RSD (%)
Wine sample	5.00	5.10	102.00	2.6
	10.00	10.80	108.00	4.6
	15.00	14.95	99.70	3.8

4. CONCLUSION

In summary, we report a facile mechanochemical synthesis of ZnO nanostructured materials for the selective electrochemical detection of GA. The HP-ZnO modified electrode shows an excellent detection limit, good linear range, cheap, rapid response with good reproducibility. The common interfering compounds, such as CT, DA, CA, MR, HQ, UA, AA, FA and AC present in the real samples did not show any interference in the determination of GA. Moreover, the proposed sensor was successfully applied in the determination of GA in wine samples.

ACKNOWLEDGEMENTS

The authors gratefully acknowledge the financial support of the National Taipei University of Technology, and Mackay Memorial Hospital Joint Research Program (NTUT-MMH-108-06 and MMH-TT-10807). The project was supported by the Ministry of Science and Technology (MOST), Taiwan. We would also like to acknowledge The Ministry of Science and Technology, Taiwan (MOST 107-2113-M-027 -005 -MY3) and MacKay Memorial Hospital, Taipei, Taiwan (NTUT-MMH-108-06) for its financial support.

References

1. Y. L. Su and S. H. Cheng, *Anal. Chim. Acta*, 901 (2015) 41–50.
2. L. P. Souza, F. Calegari, A. J. G. Zarbin, L. H. M. Júnior, and M. F. Bergamini, *J. Agric. Food Chem.*, 59 (2011) 7620–7625.
3. A. T. E. Vilian, J. Y. Song, Y. S. Lee, S. K. Hwang, H. J. Kim, Y. S. Jun, Y. S. Huh, Y. K. Hana, *Biosens. Bioelectron.*, 117 (2018) 597–604.
4. Y. Gao, L. Wang, Y. Zhang, L. Zou, G. Li, and B. Ye, *Anal. Methods*, 8 (2016) 8474–8482.
5. J. Tashkhourian, S. F. N. Ana, S. Hashemnia, and M. R. Hormozi-Nezhad, *J. Solid State Electrochem.*, 17 (2013) 157–165.
6. R. A. Hamid and E. F. Newair, *J. Electroanal. Chem.*, 704 (2013) 32–37.
7. J. Tashkhourian and S. F. Nami-Ana, *Mater. Sci. Eng. C*, 52 (2015) 103–110.
8. S. M. Ghoreishi, M. Behpour, M. Khayatkashani, and M. H. Motaghedifard, *Anal. Methods*, 3 (2011) 636–645.
9. N. Raja, T. Kokulnathan, S. M. Chen, W. C. Liao, and T. Sakthi Priya, *Int. J. Electrochem. Sci.*, 12 (2017) 4620–4629.
10. Z. Liang, H. Zhai, Z. Chen, H. Wang, S. Wang, Q. Zhou, X. Huang, *Sensors Actuators, B Chem.*, 224 (2016) 915–925.
11. C. Xiong, Can Xionga,1, Yang Wangb,1, Hao Qub,*, Lijun Zhanc, Longzhen Qiuc, Wei Chena, Feng Yand, Lei Zheng., *Sensors Actuators, B Chem.*, 246 (2017) 235–242.
12. F. Gao, D. Zheng, H. Tanaka, F. Zhan, X. Yuan, F. Gao, Q. Wang, *Mater. Sci. Eng. C*, 57 (2015) 279–287.
13. M. Ghaani, N. Nasirizadeh, S. A. Yasini Ardakani, F. Z. Mehrjardi, M. Scampicchio, and S. Farris, *Anal. Methods*, 8 (2016) 1103–1110.
14. T. Kokulnathan, S.-M. Chen, *ACS Sustain. Chem. Eng.*, 7, (2019) 4136–4146.
15. T. Kokulnathan, R. Manikandan, S. M. Chen, and V. K. Ponnusamy, *J. Taiwan Inst. Chem. Eng.*, 93 (2018) 11–20.
16. S. Sakthinathan, T. Kokulnathan, S. M. Chen, T. W. Chen, T. W. Tseng, X. Liu, W. C. Liao, *Int. J.*

- Electrochem. Sci.*, 12 (2017) 6829–6841.
17. T. Kokulnathan, N. Raja, S.-M. Chen, R. Sukanya, and B. Thirumalraj, *J. Electrochem. Soc.*, 164 (2017) H958–H966.
 18. T. Kokulnathan, S. Sakthinathan, S. M. Chen, R. Karthik, and T. W. Chiu, *Inorg. Chem. Front.*, 5 (2018) 1145–1155.
 19. T. Kokulnathan, T. S. K. Sharma, S.-M. Chen, and Y. Han-Yu, *J. Electrochem. Soc.*, 165 (2018) B281–B288.
 20. P. Rai, W. K. Kwak, and Y. T. Yu, *ACS Appl. Mater. Interfaces*, 5 (2013) 3026–3032.
 21. S. Tiwari, M. Vinchurkar, V. R. Rao, and G. Garnier, *Sci. Rep.*, 7 (2017) 1–10.
 22. A. Khataee, A. Karimi, S. Arefi-Oskoui, R. D. C. Soltani, Y. Hanifehpour, B. Soltani, S. W. Joo, *Ultrason. Sonochem.*, 22 (2015) 371–381.
 23. H. Köse, Ş. Karaal, A. O. Aydın, and H. Akbulut, *J. Power Sources*, 295 (2015) 235–245.
 24. E. Manova, T. Tsoncheva, D. Paneva, M. Popova, N. Velinov, B. Kunev, K. Tenchev, I. Mitov, *J. Solid State Chem.*, 184 (2011) 1153–1158.
 25. S. Dhara and P. K. Giri, *Appl. Nanosci.*, 1 (2011) 165–171.
 26. K. Lingaraju, H. Raja Naika, K. Manjunath, R. B. Basavaraj, H. Nagabhushana, G. Nagaraju, D. Suresh, *Appl. Nanosci.*, 6 (2016) 703–710.
 27. Z. Lazarevic', C'. Jovalekic', A. Rec'nik, V.N. Ivanovski, A. Milutinovic', M. Romc'evic', M.B. Pavlovic', B. Cekic', N.Z'. Romc'evic', *J. Materresbull*, 48 (2013) 404–415.
 28. T. Kokulnathan, A. Joseph Anthuvan, S. M. Chen, V. Chinnuswamy, and K. Kadirvelu, *Inorg. Chem. Front.*, 5 (2018) 705–718.